Materials
Advances

Accepted Manuscript

This article can be cited before page numbers have been issued, to do this please use: K. Rafiq, Z. Abid, K. Aljohani, B. S. Aljohani, M. Jalil, S. Andleeb and E. Hussain, *Mater. Adv.*, 2026, DOI: 10.1039/D6MA00439C.

View Article Online
DOI: 10.1039/D6MA00439C

ARTICLE

Scientific insight into the dual role of Cu–cocatalysts for electron injection onto schottky junctions: sunlight driven H_2 production with Cu@Si–CdS system†

Received 00th January 20xx,
Accepted 00th January 20xx

DOI: 10.1039/x0xx00000x

Khezina Rafiq[ab], Muhammad Zeeshan Abid[ac], Khalid Aljohani[d], Bassam S. Aljohani[e], Muhammad Jalil[a], Sohaila Andleeb[f], Ejaz Hussain[ag]*

Current work reveal the successful synthesis of Cu@Si–CdS catalysts and their application in sunlight–driven hydrogen generation. Hydrothermal approach was employed to achieve the required characteristics and compositional characteristics, while the synthesis reactions were carefully controlled to ensure precise silicon doping and uniform copper loading. To assess optical and structural characteristics of catalysts analytical techniques such as, XRD, SEM, AFM, UV–Vis/DRS, FT–IR, PL, Raman and VSM have been employed and justified. Photoelectrochemical experiments (i.e., photocurrent and elctron impedence measurements were conducted to confirm the charge separation andtransfer onto the active sites. EDX and XPS techniques were used to confirm the purity and chemical compositions. Photoreactions were carried out in 140 mL glass reactor (Velp-Sci), whereas hydrogen evolution was monitored via gas charamatography equiped with thermal conductivity detector (GC–TCD). Catalytic activities, i.e. hydrogen evolution performances, indicated that Cu@Si–CdS catalysts deliver 23.85 mmol g^{-1} h^{-1} of hydrogen. This activity is six times higher than that of pristine CdS or catalysts lacking Si dopants and Cu cocatalysts. Superior activities of Cu@Si–CdS catalysts is ascribed to presence of silicon dopants and localized surface plosmon resonance (LSPR) of Cu–cocatalysts. During photoreactions, Si dopants generates additional energy levels, resulting extended light absorption capability of catalysts. Additionally, metal cocatalysts (i.e. Cu in present work) develop schottky junctions that facilitates the rectification of charges onto the active sites and restrict recombinations. To determine the optimal conditions, various factors including temperature, pH, light intensity and catalyst dose were precisely assessed and optimized. These results demonstrates that Cu@Si–CdS catalysts system hold significant potentially for sustainable hydrogen production.

Introduction

It is quite important to realize that due to substantial increasing of industrialization and urbanization over the past few years, energy demands have been increased excessively[1]. Although there exist other options however 78% of energy requirements are still compensated by the conventional sources i.e. fossil fuels. Significant drawback associated with fossil fuels is that they are rapidly diminishing due to their huge and excessive demands[2]. Another drawback of fossil fuel-based energy sources is their significant contribution to greenhouse gas emissions[3]. These greenhouse gases then cause atmospheric pollution and global warming. To tackle the environmental as well as energy related issues, hydrogen has been proven to be the most auspicious and reliable fuel that can potentially solve the aforementioned issues[4].

One of the key advantages of hydrogen is that it is regarded as a clean and sustainable energy carrier within the framework of renewable energy systems. Another important benefit is that its oxidation (combustion) releases a high specific enthalpy (ΔH) while producing net-zero carbon emissions[5]. Consequently, hydrogen has strong potential to serve as an alternative fuel to replace conventional fossil fuels. However, molecular hydrogen does not occur freely in nature

a. Institute of Chemistry, Inorganic Materials Laboratory 52S, The Islamia University of Bahawalpur–63100, Pakistan.
b. Shimmer Center, Tianfu Jiangxi Laboratory, Chengdu, 641419, P.R. China.
c. College of Chemistry and Molecular Sciences, Henan University, Kaifeng, 475004, PR China.
d. Department of Mechanical Engineering, College of Engineering in Al-Kharj, Prince Sattam Bin Abdulaziz University, Al-Kharj, 11942, Saudi Arabia.
e. Department of Mechanical Engineering, College of Engineering, Taibah University, Yanbu, 41911, Saudi Arabia.
f. Institute of Chemistry, University of Sargodha, Sargodha Pakistan.
g. International Center for Interdisciplinary Research in Sciences (ICIRS), The University of Lahore, Lahore, Pakistan.
Corresponding authors: ejaz.hussain@iub.edu.pk
Dedication: In the loving memory of Maryam Ashraf who was an active member of Lab 52s.
†Supplementary Information available. See DOI: 10.1039/x0xx00000x

View Article Online
DOI: 10.1039/D6MA00439C

and must be generated from renewable feedstocks such as water and biomass[6]. Hydrogen production can be achieved through several routes, including biophotolysis, electrolysis and thermolysis of water, hydrocarbon pyrolysis, steam reforming and catalytic water splitting[7, 8]. Among these approaches, photocatalytic water splitting is considered one of the most efficient and promising methods for sustainable hydrogen generation. To date, a wide range of semiconductor materials–such as metal oxides, metal sulphides, chalcogenides, metal ferrites and vanadates, graphitic carbon nitride, graphene and graphene-supported catalysts, metal–organic frameworks (MOFs), covalent organic frameworks (COFs), and polyoxometalates (POMs)–have been extensively investigated for water-splitting applications[9-19].

Significant drawbacks associated with above mentioned catalysts are: (i) poor stability due to structural defects (ii) lower efficiencies due to large band gaps (iii) photo corrosion and fast charge recombination (iv) minimum light absorption and yield (v) high cost and low scalability (vi) low active sites (vii) incompatibility with reaction media (i.e. water). For example, TiO_2 has large bandgap due to which it can works only in ultraviolet light[20]. These are the significant reasons; researchers have shown great interest in developing visible light catalysts. Nevertheless, there have been reported numerous catalysts, but CdS is a semiconductor catalyst that has great potential to split water in the presence of visible light[21]. Advantage is that CdS is a moderate bandgap catalyst and can be successfully tuned with transition metal cocatalysts[22, 23]. Relative

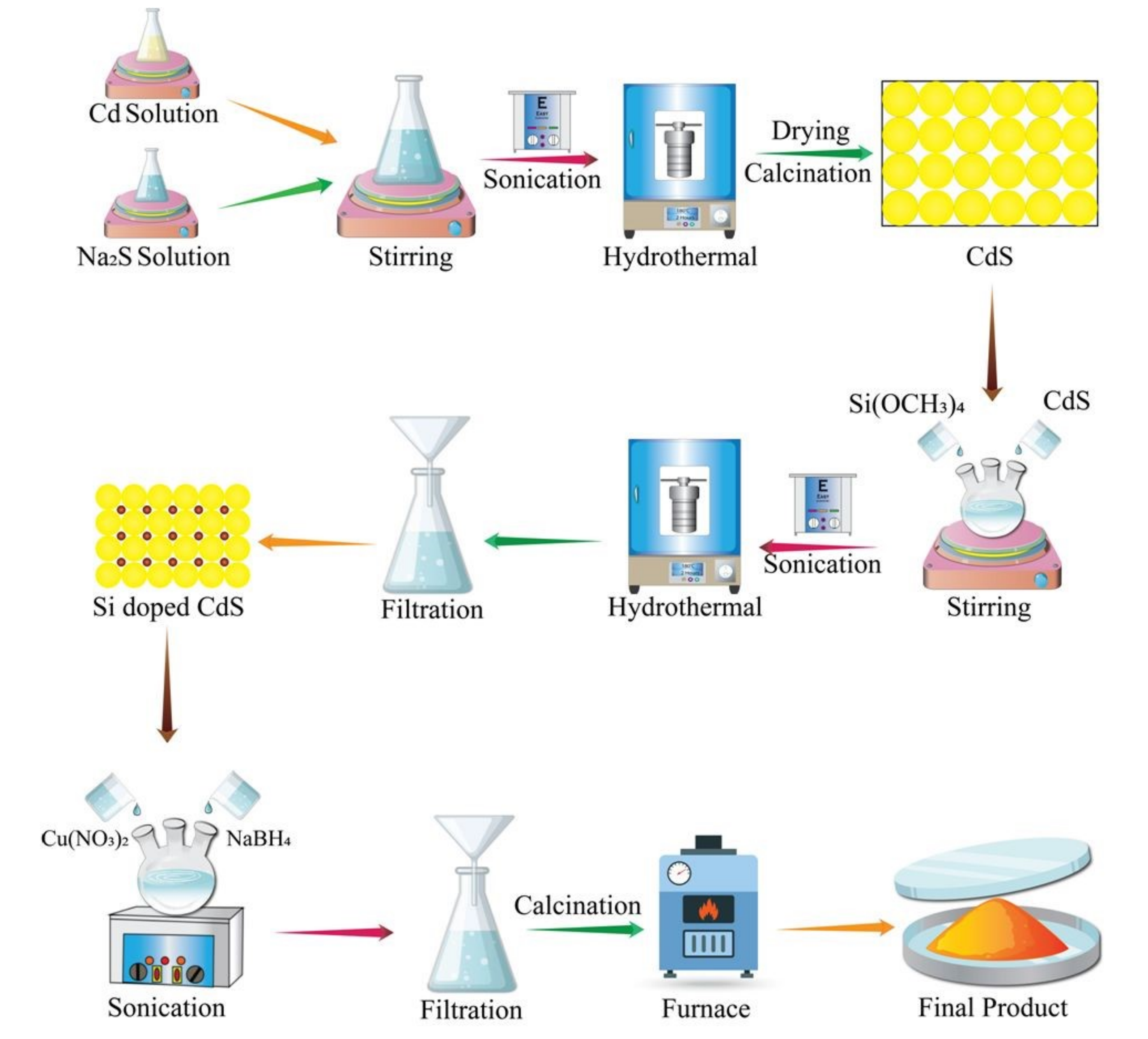

Fig. 1: Schematic diagram illustrating the synthesis of Cu@Si–CdS catalysts.

View Article Online
DOI: 10.1039/D6MA00439C

to the other semiconductor systems, it is quite suitable for photocatalytic water splitting because it possesses excellent light absorbance capability, low resistivity and better photoconductivity[24]. Despite the fact that it is excellent catalyst but significant drawback associated with CdS is that it readily decomposed during the photoreaction. However, stability and catalytic efficiency of CdS can be enhanced by modifying its morphology through the development of heterostructures i.e. silicon doping and cocatalysts loading[25]. Catalyst's morphology and surface area is crucial factor that switch its optical, electrical and catalytic performances. Recently several studies have been reported and proved that CdS hybrid structures such as MXenes/CdS, COFs/CdS, MOFs/CdS and transition metal loaded or doped CdS catalysts have potential to generate hydrogen from water splitting reaction[26-29]. Numerous reports indicated that metal loading or doping is more preferable than heterostructures because metals exhibit high stability and activity for photocatalytic reactions[30]. Furthermore, metal loading or doping on CdS structures effectively raises the fermi levels by suppressing charges recombination[31].

Localized surface plasmon resonance (LSPR) is an electronic effect predominantly observed in noble metals such as Au, Ag, and Cu and has been shown to significantly improve catalytic performance in photocatalytic processes[32]. Copper and gold cocatalysts exhibit LSPR phenomenon upon visible irradiations[33, 34]. In current work, Cu cocatalyst has been selected due to its commercial availability, easy accessibility and relatively low cost[35, 36]. Several studies have illustrated the LSPR effect of Cu over metal oxide or sulphide semiconductors[37]. Moreover, copper metal has attracted considerable attention not only due to its high stability, conductivity and catalytic activity, but also because it can simultaneously function as an electron trapping cocatalysts and visible-light responsive plasmonic material during photocatalytic reactions. The deposition of Cu cocatalysts on the CdS surface may promote Schottky-type interfacial interactions, which facilitate electron migration and

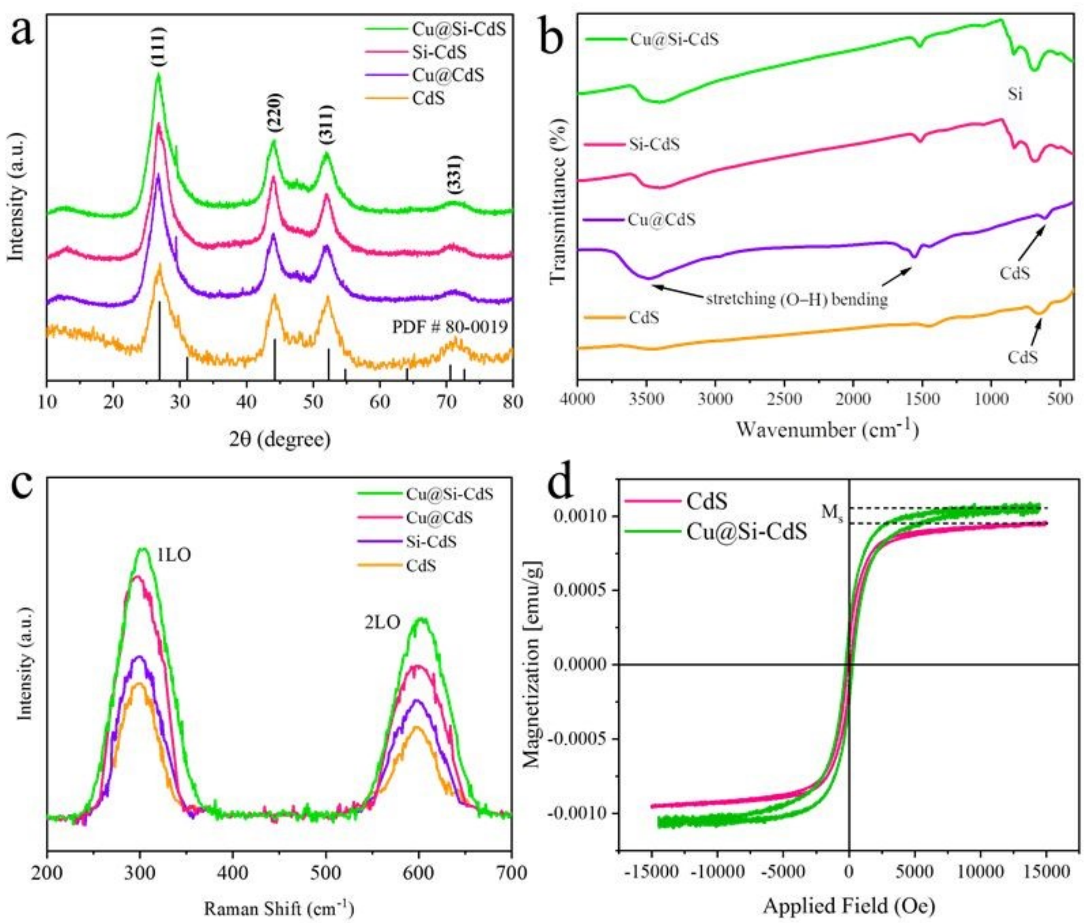

Fig. 2: Illustrate (a) represents XRD results, (b) FTIR, (c) Raman analysis and (d) represent the VSM analysis of Cu@Si–CdS catalysts.

View Article Online
DOI: 10.1039/D6MA00439C

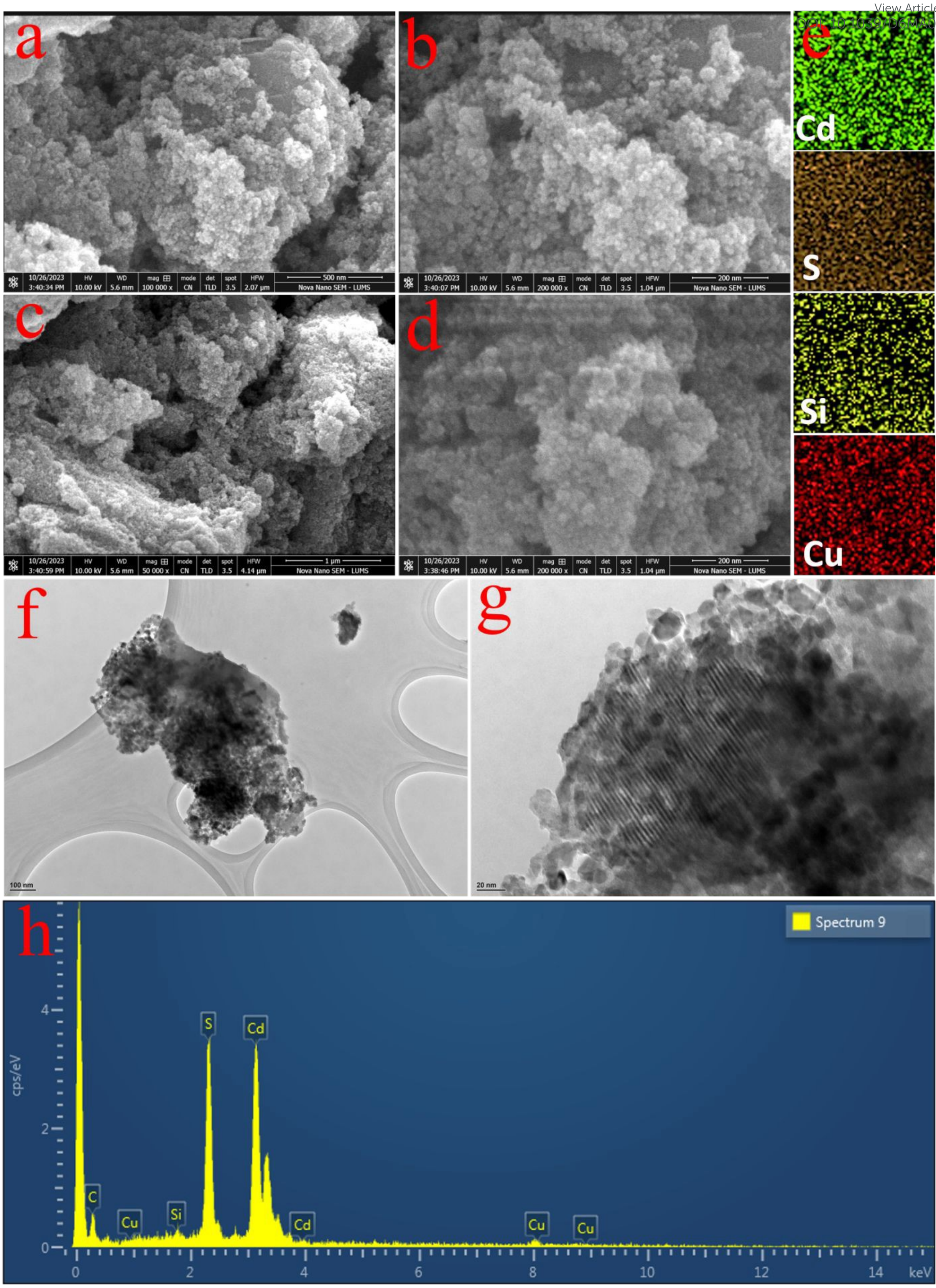

Fig. 3: SEM results of pure CdS (a) 500 nm (b) 200 nm, Cu@Si–CdS results at (c) 1 µm (d) 200 nm and (e) show mapping images of Cd, S, Si and Cu, (f & g) represent the TEM micrographs whereas (h) shows the EDX spectrum of Cu@Si–CdS catalysts.

suppress electron back-transfer interfacial interactions, which facilitate electron migration and suppress electron back transfer during photocatalytic reactions[38]. In addition, Si incorporation into the CdS lattice enhances its electrical conductivity and may introduce defect-mediated energy states, thereby facilitating more efficient electron transport and charge separation at the catalytic active sites[39, 40]. The synergistic interaction between Cu cocatalysts and Si dopants is expected to improve visible light utilization, accelerate interfacial charge transfer and suppress charge carrier recombination within the CdS system.

Building on the above advantages, Cu@Si–CdS photocatalysts were designed and systematically evaluated for photocatalytic hydrogen evolution. Copper cocatalysts were directly anchored onto Si-doped CdS through an in-situ chemical reduction route. Among the prepared samples, the $Cu_{2.0}$@Si–CdS composition exhibited the highest photocatalytic performance, achieving a hydrogen evolution rate of 23.85 mmol g^{-1} h^{-1}. The enhanced activity is attributed to plasmon-induced hot electron generation from the Cu co-catalysts, which increases electron density at the reactive sites of Si–CdS. Furthermore, the establishment of Schottky interfaces at the Cu/Si–CdS junctions effectively inhibits charge carrier recombination, thereby promoting efficient charge utilization.

Experimental

View Article Online
DOI: 10.1039/D6MA00439C

Chemicals and equipment along with detailed have been discussed in the supporting information (ESI) Section.

Synthesis of catalysts

CdS, Si–CdS and Cu@Si–CdS catalysts were synthesized using a hydrothermal method[41]. In a typical procedure, 2.75 g of $Cd(NO_3)_2.4H_2O$ was dissolved in 50 mL of double-distilled water. The two solutions were than combined in a three-neck round-bottom flask and continuously stirred magnetically for 5 h. To ensure uniform dispersion, the resulting suspension was subjected to sonication, after which the CdS precipitates were transferred into an autoclave reactor. The autoclave was heated in an oven at 170 °C for 3 h. The resulting pale-yellow precipitate was recovered by vacuum filtration and thoroughly washed with distilled water followed by absolute ethanol. After drying, the CdS catalyst was calcined in a muffle furnace at 350 °C[42].

To prepare Si–CdS, 250 mg of as-synthesized CdS powder were dispersed in 30 mL of distilled water whereas mixture was stirred continuously to obtain CdS slurry. For doping of Si, 34 mg of

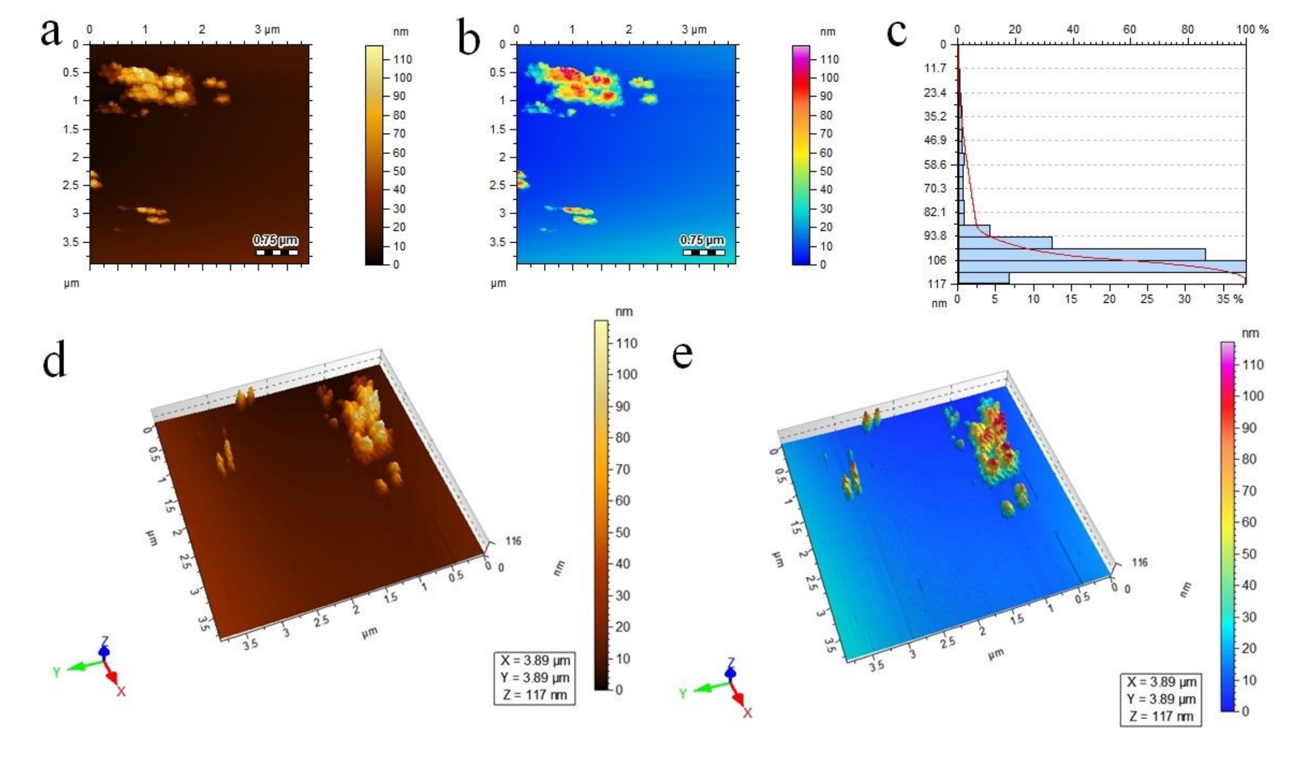

Fig. 4: (a & b) represents the 2D topographic images, (c) illustrate height scale and (d & e) shows 3D topographic images of Cu@Si–CdS catalysts.

View Article Online
DOI: 10.1039/D6MA00439C

tetramethoxysilane ($Si(OCH_3)_4$) was transferred to aforementioned slurry with genteelly stirring for 2h before hydrothermal reaction[43, 44]. After completing hydrothermal treatment, yellow precipitates of Si–CdS catalyst were collected by vacuum filtration. Catalysts were then dried at 65 ℃. Utilizing three-neck reaction flask, Si–CdS catalyst was subjected for Cu cocatalysts fabrication. For Cu loading, $Cu(NO_3)_2.3H_2O$ salt was used as a precursor source. After stirring 1h, $NaBH_4$ solution was used to reduce the Cu^{2+} ions. Precipitates of Cu@Si–CdS catalysts were recovered via vacuum filtration. After calcination, catalysts were preserved for photoreactions (catalytic activities) and necessary characterizations. Synthesis scheme of catalysts used in current work is presented in the Fig.1.

Hydrogen-evolution experiments

Photocatalytic hydrogen evolution reactions were conducted in the presence of sunlight from 10am to 4pm in the clear sky at the location 29.377425° N, 71.759386° E, in the month of June-2023. Photon flux reaching the sample surface was (e.g., 700 W/m²). For photoreaction, 20 mg of photocatalyst was transferred in a 5% ethanol solution (net volume 25 mL), in 140 mL glass reactor[45]. Prior to the photoreaction, high-purity nitrogen gas was purged from reaction mixture. This was done to remove the dissolved oxygen contents form mixture[46]. Flow rate of the nitrogen was maintained at 12 mL/min for 3 h. Using Extech LT300, light intensity was measured as 800 W/m^2[47]. Syringe (half mL) was used to collect gas samples from headspace of photoreactor[48]. The collected gas samples were analysed using gas chromatography equipped with a thermal conductivity detector (GC–TCD) and a molecular sieve capillary column. Quantitative determination of hydrogen

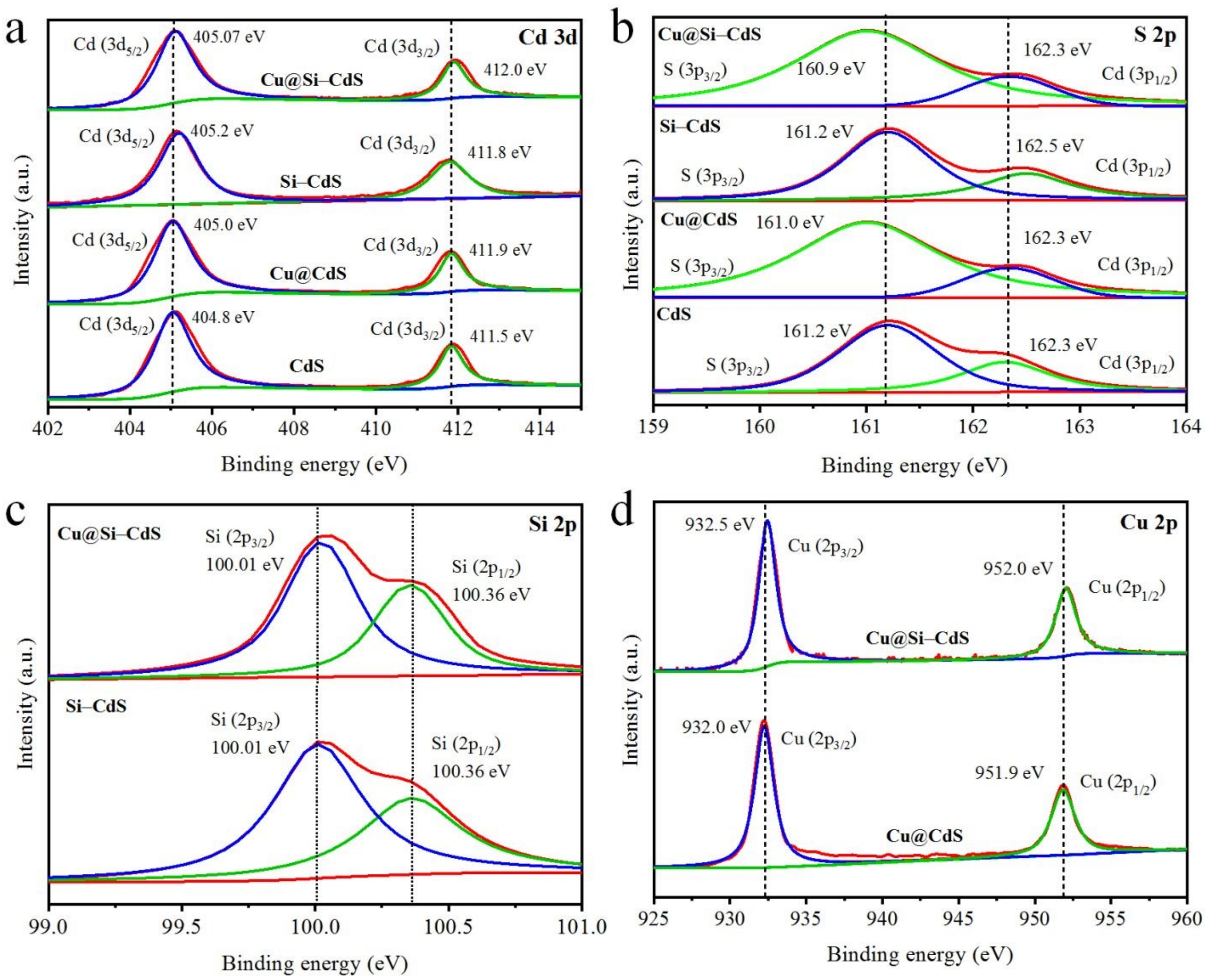

Fig. 5: (a) XPS analyses of Cd 3d (b) S 2p, (c) Si 2p and (d) represents the XPS of Cu, for pristine CdS, Si–CdS, Cu@CdS and Cu@Si–CdS catalysts.

View Article Online
DOI: 10.1039/D6MA00439C

production was carried out using an internally calibrated standard curve[48]. To verify the reproducibility and reliability of the catalysts, each photocatalytic experiment was performed at least three times. Hydrogen evolution rates were expressed in units of mmol g^{-1} and mmol g^{-1} h^{-1}, and the photocatalytic performances of different materials were compared under identical experimental conditions[49]. The apparent quantum yield of the photoreaction was calculated using the equations provided below[50].

$$\text{Q.E} = \frac{\text{number of reacted electrons}}{\text{number of incidents photons}} \text{ x } 100\ \% \quad \textbf{(1)}$$

$$\text{Q.E} = \frac{2 \text{ x number of evoluted } H_2 \text{ molecules}}{\text{number of incidents photons}} \text{ x } 100\% \quad \textbf{(2)}$$

Results and discussions

Fig.1 depicts the synthesis technique for both CdS and Cu@Si–CdS photocatalysts, and has comprehensively discussed in experimental section of this study. Results obtained various characterization techniques have been discussed with precision and accuracy.

XRD analysis

XRD pattern of as-prepared catalysts were conducted to evaluate the structure and crystallinity[51]. Results were recorded on between 10°–80° range, as illustrated in Fig. 2(a). Major diffraction patterns were identified at specific angles: 26.54°, 44.03°, 52.16° and 70.59°, and each pattern were distinguished with hkl values (111), (220), (311) and (331), respectively. Crystal planes are exactly matched with the JCPDS #80−0019 [52] which corresponds to cubic CdS. Results revealed that due to low concentrations and high dispersion of Cu cocatalysts, no significant changes in the diffraction pattern were observed after

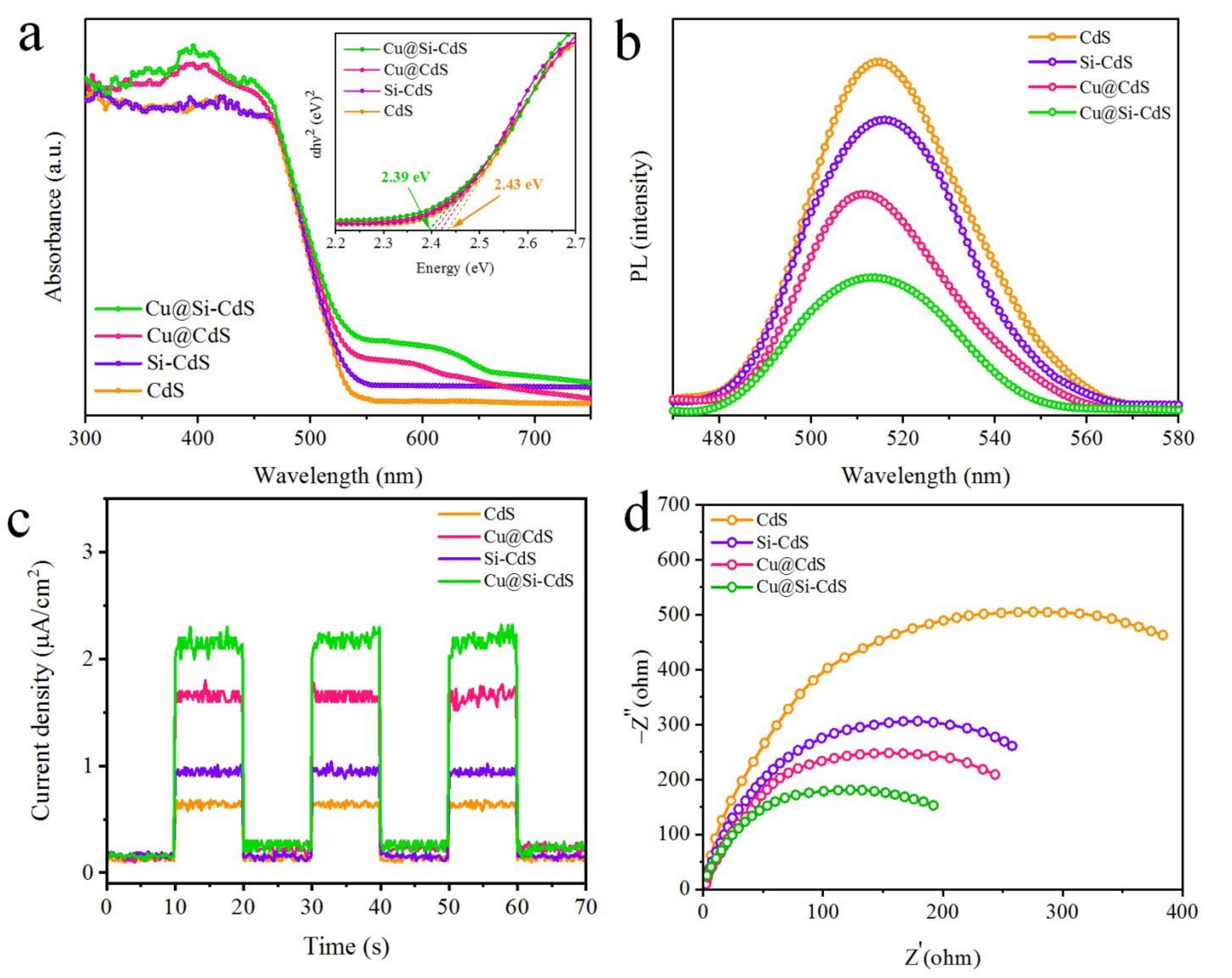

Fig. 6: (a) UV–Vis/DRS measurements (inset; optical bandgap calculation using Tauc plot method), (b) Photoluminescence results, (c) photocurrent response and (d) represents EIS results of pristine CdS, Si–CdS, Cu@CdS and Cu@Si–CdS catalysts.

View Article Online
DOI: 10.1039/D6MA00439C

Cu loading. Furthermore, no additional impurity peaks corresponding to Cu or copper oxide phases were detected, suggesting that the cubic CdS crystal structure and phase purity were well preserved. The absence of major peak shifts or broadening also indicates that Cu incorporation did not significantly disturb the crystallinity of the CdS lattice.

FTIR and Raman analyses

FTIR results have been illustrated in Figure 2(b), it has been investigated that FTIR spectrum of CdS exhibits characteristic stretching vibration at 647 cm^{-1}[34]. Results exhibit broad band bending vibrations at 3451 cm^{-1}, while stretching vibrations observed at 1616 cm^{-1} attributed to the surface hydroxyl groups of adsorbed water molecules. On the other hand, presence of sharp peak at 820 cm^{-1} assures Si–CdS bond vibrations[53]. Results indicated that Cu metal is exist over the surfaces and hasn't exhibits any vibrations. Raman results of as prepared catalysts are presented in the Fig. 2(c). In the Raman spectrum, it can be clearly seen that two major vibrations modes indicated at 300 and 600 cm^{-1} associated with CdS phonon modes[54]. It has been observed that for pure CdS catalyst, intensity of Raman peaks is relatively low as compared to surface–enhanced Raman scattering that arose due to Si dopants and Cu loading[55, 56].

Vibrating sample magnetization (VSM)

Magnetic properties of the Cu@Si–CdS catalysts were evaluated by vibrating sample magnetization. This analysis was performed to investigate the influence of Cu cocatalyst loading and Si doping on the electronic structure and charge transfer properties of the CdS system. VSM curve of Cu@Si–CdS catalysts approaches the saturation point (M_s) rapidly. In magnetic profile of catalysts, absence of strong hysteresis loop suggests that catalysts have less

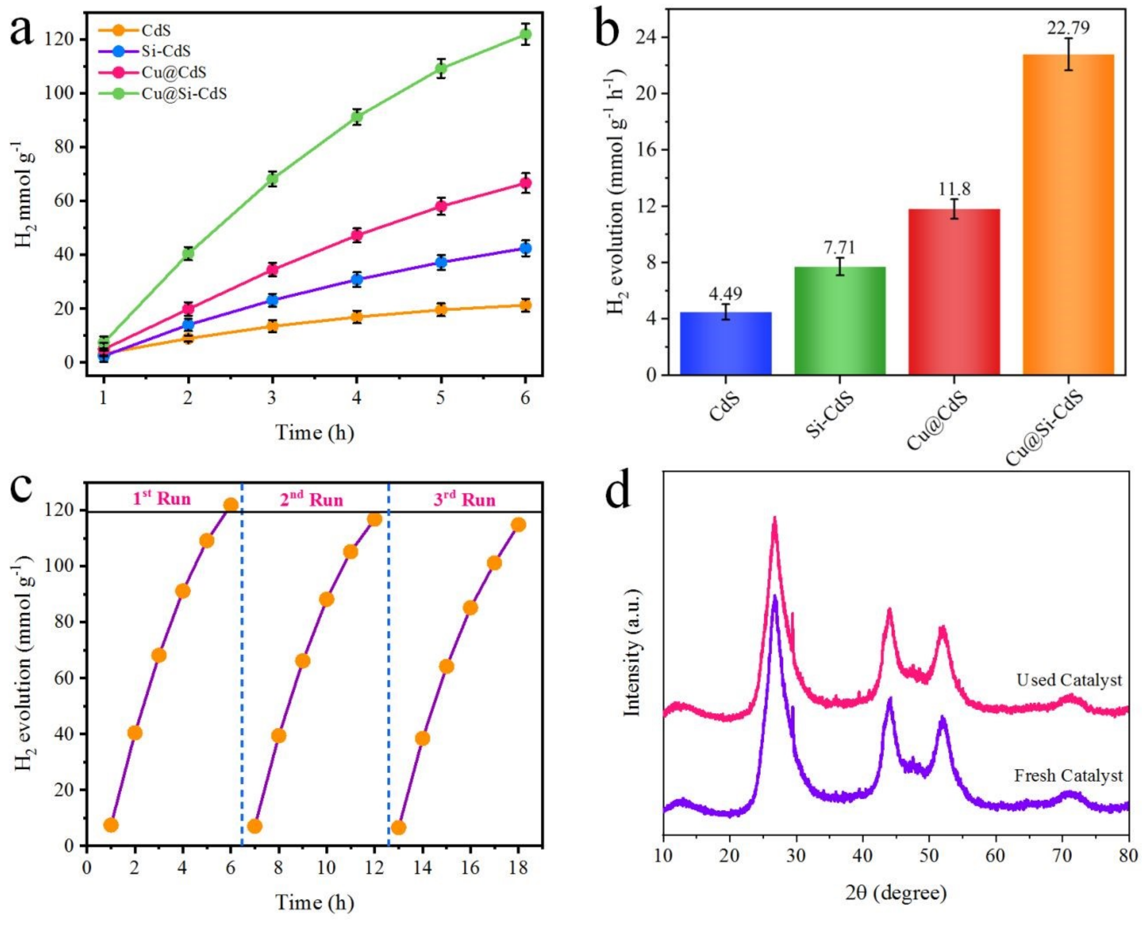

Fig. 7: Activities of Cu@Si–CdS (a) represents in mmol g^{-1}, (b) illustrate in mmol g^{-1} h^{-1}, (c) recyclability test and (d) XRD of Cu@Si–CdS after photoreaction.

View Article Online
DOI: 10.1039/D6MA00439C

magnetic behaviour, see results in Fig. 2(d). Observed magnetization (M_s) value of as synthesized catalysts was 0.009 emu/g. Generally, magnetization of materials depends upon particle sizes of the materials. For example, if size of nanoparticles is small then it will exhibit less magnetic properties[57]. Langevin law was used to measure the saturation point of the materials[58]. CdS itself is diamagnetic material while the doping of Si and loading of Cu develop some magnetic properties in the Cu@Si–CdS catalysts and indicative of successful synthesis of catalysts (vide infra). Cu induces a slight ferromagnetism and increases Ms in CdS. These modifications facilitate improved interfacial electron transfer across the Cu-induced Schottky junctions, suppress charge recombination, and consequently enhance photocatalytic hydrogen generation performance.

SEM, TEM and EDX Analyses

SEM, TEM and EDX results of as-synthesized CdS and Cu@Si–CdS photocatalysts are revealed in Fig. 3. SEM results of pristine CdS at 500 and 200 nm revealed a homogeneous morphology of the photocatalysts [Fig. 3(a & b)]. They have uniform morphology with high degree of purity confirmed by EDX (Fig. S1). Whereas SEM results of Cu@Si–CdS photocatalysts have relatively more uniform and nano spherical shaped particles [Fig. 3(c & d)]. Results obtained from EDX spectroscopy revealed the elemental composition of Cu@Si–CdS photocatalysts, in which all essential elements of the catalysts i.e., Cd, S, Cu and Si were detected and confirmed. The EDX mapping depicted in Fig. 3(e), displays the elemental distribution within the catalysts.

For analysing the internal morphology of as-synthesized catalysts transmission electron microscopic (TEM) analysis of catalysts was performed. Two TEM micrographs of catalysts at various magnifications (i.e. 100 nm & 20 nm) have been shown in Fig. 3 (f & g). TEM micrographs assure the agglomeration of CdS particles as shown in SEM images. TEM analysis also confirms the uniform distribution of Cu cocatalysts over the CdS surfaces. Si doping does not alter the CdS internal structure but creates structural defects at external sites of CdS, which provide more reaction sites for catalytic reactions to produce H_2 [59]. In EDX graph [Fig. 3(h)] no extra peak was observed which confirm the successful preparation and purity of catalysts. These results validate the effectiveness of the synthesis strategy in producing high-purity Cu@Si–CdS photocatalysts with a uniform morphology. These properties are essential for achieving high photocatalytic performance. In other words, Cu@Si–CdS photocatalysts are well established and have the desired properties for use of water splitting reaction[60].

Atomic Force Microscopic results of Cu@Si–CdS

Atomic force microscopic results of Cu@Si–CdS catalysts have been demonstrated in Fig. 4 that provide valuable insights into the surface topography and particle size distribution[61]. AFM results revealed that, Cu@Si–CdS nanostructures exhibit highly dispersed and uniform morphology. Fig. 4(a, b) represents the 2D topography of the catalysts. Particle size distributions have been revealed in Fig. 4c, ranging from 0.5 nm to 117 nm. Average particle height was observed to be 106 nm. The topography of catalysts is revealed in 3D images with a scan area of 3.89 × 3.89 µm, as shown in Fig. 4(d, e). The RMS roughness is 8.2 nm, indicating a relatively uniform surface morphology with the majority of nanostructures in the height range of 93–117 nm. Overall, AFM analysis reveals that Cu@Si–CdS nanostructures have a uniform morphology and size. These properties are essential for achieving high photocatalytic performances[62, 63].

XPS studies

X–ray photon spectroscopic studies were conducted to investigate the purity, oxidation state, composition, and electronic interactions between elements of pristine CdS, Si–CdS, Cu@CdS and Cu@Si–CdS catalysts. Binding energies observed for cadmium (Cd), sulfur (S), copper (Cu) and silicon (Si) have been shown in Fig. 5[64]. Two peaks corresponding to the Cd 3d electrons have been observed at 404.8 eV and 411.5 eV for $3d_{5/2}$ and $3d_{3/2}$ that signifies Cd bond with sulfur in CdS, these peaks are separated by 6.7 eV. Results indicate that cadmium exist in the +2-oxidation state, Fig. 5(a). In case of Cu@CdS and Si–CdS, these peaks were slightly shifted towards the higher binding energies, that confirms the interaction between them[33]. A doublet was observed that appears at 161.2 and 162.3 eV corresponds to the $2p_{3/2}$ and $2p_{1/2}$, indicate that sulfur is in –2 oxidation state, see Fig. 5(b)[65]. Whereas, for Cu loaded and Si doped samples these energies were slightly shifted towards lower binding energies. Similarly, for Si–CdS and Cu@Si–CdS catalysts, two peaks

View Article Online
DOI: 10.1039/D6MA00439C

were observed for Si $2p_{1/2}$ and $2p_{3/2}$ at 100.36 and 100.01 eV, Fig. 5(c)[66]. Fig. 5(d) shows Cu XPS results for Cu@CdS and Cu@Si–CdS catalysts. For Cu@CdS, the two prominent peaks at 952.9 and 932.0 eV correspond to Cu $2p_{1/2}$ and Cu $2p_{3/2}$, respectively. Whereas, for Cu@Si–CdS these peaks were slightly transferred toward higher binding energies[33, 67]. Observed results revealed that Cu exists in metallic state that plays a vital role during the photoreaction.

UV–Vis/DRS Spectroscopic study

UV–Vis/DRS measurements of as-prepared photocatalysts have been done in order to investigate the bandgap and optical characteristics. Fig. 6(a) reveal optical properties of as prepared photocatalysts[68]. It is worth mentioning that bare CdS has a significant absorption edge at approximately 530 nm and exhibit little response to the visible region. However, Si–doped CdS indicate extended absorption in visible region; due to Si dopants, absorption extended from 530 to 540 nm approximately, resulting in a red shift in absorption. It has been investigated that increased absorbance was due to the LSPR phenomenon of Cu metal i.e., d-d transition of electrons[34]. Advantage of silicon doping is associated with reduction of band gap of CdS from 2.43 to 2.39 eV, see results Fig. 6(a)[69]. UV–Vis/DRS analysis reveals excellent optical characteristics of as–synthesized photocatalysts. Thus, changes in optical characteristics are attributed to the presence of silicon dopants and copper metal particle on the pristine CdS surfaces. It is obvious, moderate band gap potentially impact on photocatalytic properties of catalysts[70]. In summary, Cu@Si–CdS exhibit excellent catalytic properties specifically for water splitting reactions[71].

Photoluminescence (PL) Spectrum

Photoluminescence (PL) analysis of catalysts presented in Fig. 6(b) which provides valuable insights into the recombination rates and photocatalytic performance of these materials. Semiconductor materials typically exhibit two types of emissions: (i) trapped emissions that are broad and exhibit longer wavelength, (ii) excitonic emissions that are sharp and occurred near absorption edge[72]. Pure CdS exhibits a high-intensity peak, which indicates that back flow of

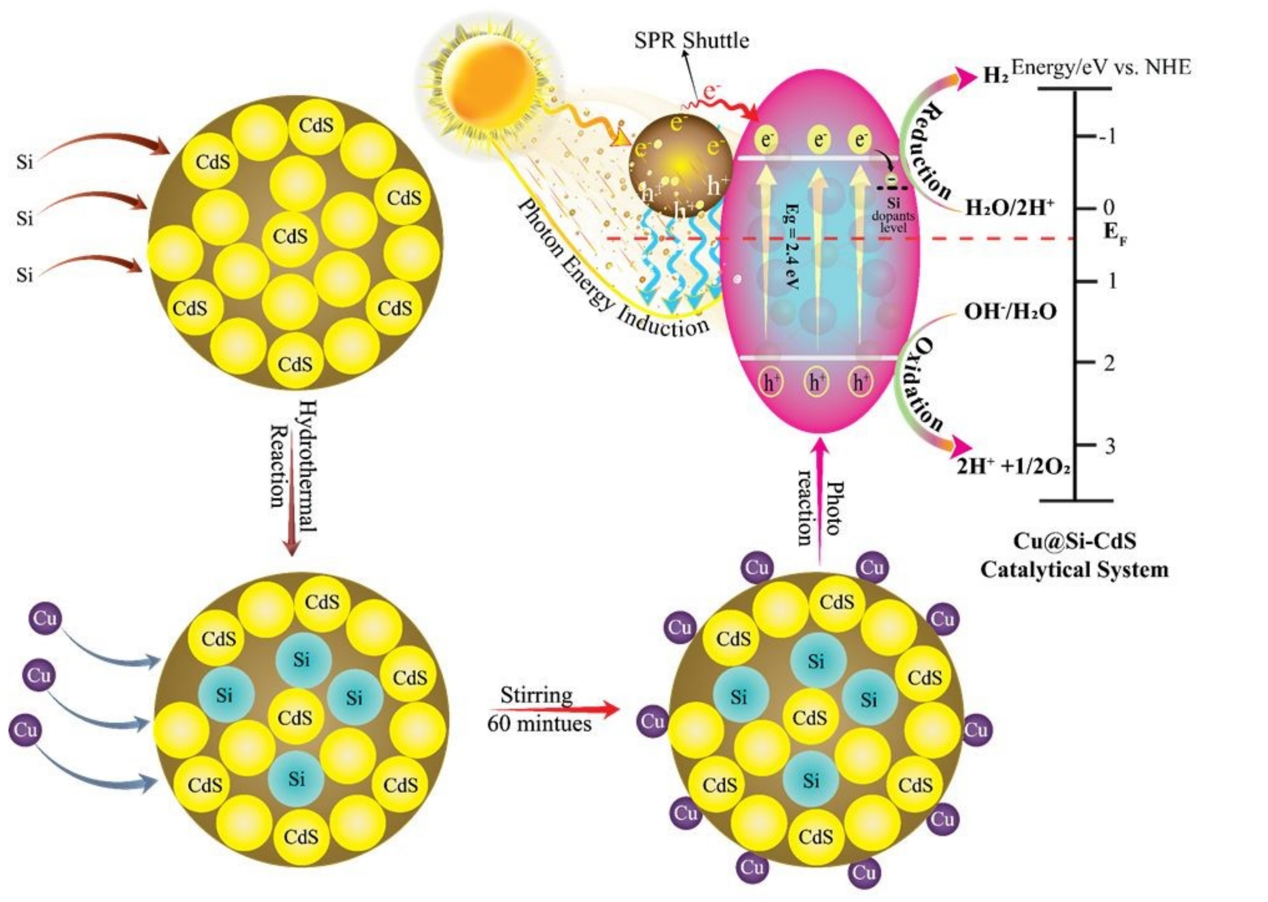

Fig. 8: Mechanism of hydrogen evolution on Cu@Si–CdS system established during photoreaction.

View Article Online
DOI: 10.1039/D6MA00439C

electrons for recombination is high. In contrast, Si doped CdS shows lower PL intensity, indicating suppressed charge recombination and improved charge transfer behaviour. Furthermore, the observed shift in PL maxima from pristine CdS to Cu@Si–CdS nanostructures may be associated with the modification of electronic structure, defect states and intermediate energy levels introduced by Si doping and Cu deposition [73] . The results obtained from PL analysis revealed the suppression of charge recombination and increment of charge transfer to the active sites for hydrogen generation. The progressive change in PL peak position also suggests altered radiative recombination pathways and interfacial electronic interactions after Cu loading and Si incorporation into the CdS system. This is because a lower recombination rate of photogenerated charges allows more efficient transfer of electrons and holes to the surface of the catalyst, where they can participate in redox reactions[74]. Overall, the PL analysis highlights the influence of Si doping and Cu deposition on the recombination behaviour, electronic structure, and photocatalytic performance of the CdS-based catalysts.

Photocurrent Response and EIS Studies

Photocurrent response and EIS analyses of photocatalysts are presented in Fig.6 (c, d). These analyses were performed to corroborate the electron-hole separation and interfacial charge transfer characteristics of Cu@Si–CdS catalysts[75]. The photocurrent response of photocatalyst is its ability to generate and transport photogenerated charges. Cu@Si–CdS exhibited a higher photocurrent density and greater stability compared to pristine CdS under visible-light irradiation. This suggests that Si–doped CdS is more efficient at separating and transferring photogenerated charges[76]. EIS is a technique used to measure the electrical impedance of a material. Arc radius in an EIS Nyquist plot represents interfacial charge transfer resistance. A lesser arc radius specifies a lower interfacial charge transfer resistance and higher efficiency in interfacial charge transfer[77]. EIS results revealed that radius of arc of Cu@Si–CdS catalysts was significantly lesser than pristine CdS; for clarification see Fig. 6(d). Overall, photocurrent response and EIS results provide strong evidence about the fact that Cu@Si–CdS has superior performance in charge separation and transfer processes compared to pristine CdS. combined results from photoluminescence (PL), photocurrent response, and EIS studies clearly demonstrate the improved electron-hole separation efficiency and interfacial charge transfer properties of Cu@Si–CdS[76]. This makes it a promising and distinct catalysts for sunlight driven water splitting reactions.

Mott-Schottky analyses

Energy bands positions (i.e., VB and CB) of CdS and Cu@Si–CdS photocatalysts were estimated using Mott–Schottky technique[78] (Fig. S2). Results demonstrated that conduction band potential (CB) of bare CdS was at –0.90 eV, while due to Si dopants and Cu cocatalysts it is –0.93 eV for Cu@Si–CdS system. With the assistance of UV–VIS/DRS and Mott–Schottky results, VB positions were calculated by **equation (3)** [79]

$$E_{VB} = E_{CB} - E_G \quad \textbf{(3)}$$

Where E_{VB} values of CdS and Cu@Si–CdS were calculated as 1.53 and 1.46 eV, respectively. These results are very supportive and justify the electron transfer mechanism of this work.

H_2 evolution activities

Cu@Si–CdS photocatalysts were assessed and evaluated for hydrogen production in the presence of visible light with 5% ethanol/water mixture that play role of sacrificial reagent[80]. For each catalyst, time of photoreaction was specified/optimised for 6 h. Initially, first photoreaction was carried out for pristine CdS that generate a poor amount of hydrogen that was 4.69 mmol g^{-1} h^{-1}. Low activity of the CdS was ascribed due to fast recombination of charges. To resolve this issue, Si metal was doped into the CdS structures and Cu metal was loaded over the surfaces of CdS. Next photoreaction was carried out for Si–CdS catalysts and it was predicted that it delivers more hydrogen than pristine or bare CdS that (7.71 mmol g^{-1} h^{-1}). Increment in activity of CdS was due to presence of Si particles in the CdS nanostructures. To evaluate the individual impact of Cu cocatalyst, H_2 evolution activity was also obtained for Cu@CdS catalysts that deliver even higher hydrogen than pristine or Si doped CdS that is 11.82 mmol g^{-1} h^{-1}. Copper is excellent cocatalysts as it exhibits inherent surface plasmon resonance phenomenon due to which it can potentially increases the catalytic efficiency. To obtained accuracy, several photocatalytic experiments were carried out to optimize the impact of Cu cocatalyst. A series of catalysts i.e., $Cu_{0.5}$@Si–CdS, $Cu_{1.0}$@Si–CdS, $Cu_{1.5}$@Si–CdS, $Cu_{2.0}$@Si–CdS and $Cu_{2.5}$@Si–CdS were prepared and evaluated for comparative

View Article Online
DOI: 10.1039/D6MA00439C

activities. These catalysts deliver 69.33, 94.81, 107.56, 121.84 and 124.16 mmol g^{-1} of hydrogen respectively, see results Fig. S3 in supporting information section. Comparative hydrogen evolution performances of all catalysts are tabulated in Table 1.

Overall, $Cu_{2.0}$@Si–CdS with 2.0 wt% Cu loading was found most active among all catalysts of this work that delivers 23.85 mmol g^{-1} h^{-1} of hydrogen. Although catalysts for higher amount of Cu cocatalysts i.e.

Table 1. Comparative hydrogen evolution activities of as prepared catalysts.

Sr. No.	*Catalysts	Cu wt% loading	Water: ethanol Ratio	H_2 generation	
				mmol g^{-1}	mmol g^{-1} h^{-1}
1	CdS	0.0	95:05	18.87	4.49
2	Si–CdS	0.0	〃	39.74	7.71
3	$Cu_{0.5}$@Si–CdS	0.5	〃	69.33	12.24
4	$Cu_{1.0}$@Si–CdS	1.0	〃	94.81	18.35
5	$Cu_{1.5}$@Si–CdS	1.5	〃	107.56	20.42
6	$Cu_{2.0}$@Si–CdS	2.0	〃	121.84	23.85
7	$Cu_{2.5}$@Si–CdS	2.5	〃	124.16	24.15

*20 mg of catalysts was used for 5% ethanol/water mixture for each photoreaction.

$Cu_{2.5}$@Si–CdS were also examined but found not much effective than $Cu_{2.0}$@Si–CdS catalysts. Results [Fig. 7 (a, b)] demonstrate excellent activity of Cu@Si–CdS catalysts, highlighting the role of Si and Cu cocatalysts for H_2 generation activity. Successive transfer of LSPR electrons of Cu cocatalysts result higher H_2 production[81]. To ensure the role of LSPR electrons, wavelength dependent experiments for the most active catalysts were assessed and optimized. Band-pass filters at various wavelengths revealed the LSPR phenomenon of Cu cocatalysts[82]. Various band pass filters such as 420 nm, 500 nm, 600 nm, and 700 nm were used to run this experiment. Activities of catalysts obtained during the photoreaction are illustrated in Fig. S4. Results indicated that H_2 production efficiency of catalysts at 600 nm was attributed to the LSPR phenomenon of Cu cocatalysts. Overall, Cu@Si–CdS photocatalysts exhibit great potential for hydrogen production applications. For more clarification, comparison of QE (%) of current work with reported literature have been provided over here; see the literature-based comparison in Table 2.

Table 2. The comparison of rate of H_2 evolution and QE (%) with reported literature.

Sr. No.	Catalyst system	Catalyst loading/ reactor volume	Illumination conditions	Sacrificial medium	H_2 evolution rate (μmol g^{-1} h^{-1})	Apparent QE (%) (λ = 420nm	Ref.
1	CdS–$Zn_{1-x}Cd_xS$	0.05 g /80 mL	Xe lamp (350 W) λ > 400 nm	Na_2S/Na_2SO_3	2300	6.3	83
2	CdS/TiO_2	0.1 g/100 mL	Xe lamp (450 W) λ ≥ 420 nm	Na_2S/Na_2SO_3	6720	4.5	84
3	NiO–CdS	0.2 g/50 mL	Xe lamp (300 W) λ ≥ 420 nm	Na_2S/Na_2SO_3	740.5	6	85
4	Sr-doped CdS	0.2 g/50 mL	Xe lamp (300 W) λ ≥ 420 nm	Na_2S/Na_2SO_3	1230	10	86
5	CdS/g–C_3N_4	0.5 g/60 mL	Xe lamp (300 W) λ > 420 nm	Methanol	4152	4.3	87
6	NiO_x/CdS	0.1 g/100 mL	Xe lamp (300 W) λ > 400 nm	Na_2S/Na_2SO_3	590.8	8.6	88
7	NiS/CdS	0.05 g/80 mL	Xe lamp (300 W) λ > 420 nm	Na_2S/Na_2SO_3	1131	6.1	89

View Article Online
DOI: 10.1039/D6MA00439C

8	CdSeZnS/ZTP	0.02 g/20 mL	Hg lamp (125 W) λ > 420 nm	Na_2S/Na_2SO_3	2142.7	9.6	90
9	Pristine CdS	0.005 g/25 mL	Natural sunlight λ ≥ 420 nm	Ethanol	4490	1.28	Present study
10	Si-doped CdS	0.005 g/25 mL	Natural sunlight λ ≥ 420 nm	Ethanol	7710	2.19	Present study
11	$Cu_{0.5}$@Si–CdS	0.005 g/25 mL	Natural sunlight λ ≥ 420 nm	Ethanol	12240	3.49	Present study
12	$Cu_{1.0}$@Si–CdS	0.005 g/25 mL	Natural sunlight λ ≥ 420 nm	Ethanol	18350	5.23	Present study
13	$Cu_{1.5}$@Si–CdS	0.005 g/25 mL	Natural sunlight λ ≥ 420 nm	Ethanol	20420	5.82	Present study
14	$Cu_{2.0}$@Si–CdS	0.005 g/25 mL	Natural sunlight λ ≥ 420 nm	Ethanol	23850	6.80	Present study
15	$Cu_{2.5}$@Si–CdS	0.005 g/25 mL	Natural sunlight λ ≥ 420 nm	Ethanol	24150	6.89	Present study

Recyclability

Stability of the photocatalysts is an important factor upon which catalysts activity relies for hydrogen generation. Recyclability test for Cu@Si–CdS was performed to investigate its stability and reusability. After photoreaction, catalysts were collected and applied for recyclability test. To obtained accuracy, three concordant photoreactions were performed and their catalytic activity were compared, see results in Fig. 7(c). It was observed that after three consecutive runs, a slight decrease in catalytic efficiency was observed that was due to loss of catalyst contents during washing and recovery process[91]. For more clarification, XRD analysis was performed to reveal the structure changes in catalyst specifically after the recyclability tests. The XRD pattern of fresh and used catalyst exhibit nearly identical and well-defined diffraction peaks, indicating that the crystal structure of Cu@Si–CdS remined largely unchanged after three cyclic photoreactions; see Fig. 7(d). Furthermore, no additional impurity peaks or significant peak shifting were observed after the recyclability tests, suggesting good structural stability and phase purity of the photocatalyst during hydrogen evolution reactions.

Mechanism

Water splitting under sunlight is a promising method; hopefully it could be the game changer for energy sector. Getting hydrogen from water splitting is not easy however it can be progressively generated via photocatalysis of water. Water splitting is inherently difficult because it requires a high Gibbs Free Energy input of approximately 237.2 kJ mol^{-1}[92]. The Cu@Si–CdS catalysts developed in this study demonstrated high efficiency for solar-driven hydrogen production, which can be attributed to several contributing factors such as; (i) stability and durability of catalysts (ii) suitable band gap and band potentials (iii) presence of silicon dopants (iv) higher work function due to the presence of metal cocatalysts (v) impact of surface plasmon electrons (vi) relatively higher response in visible spectrum of sunlight[93, 94]. Fig. 8 illustrate the overall mechanistic approach for hydrogen production reaction on Cu@Si–CdS catalytic system. During photoreaction, Cu species may facilitate interfacial electron transfer towards the conduction bands of CdS i.e. semiconductor system where presence of silicon dopants establishes additional energy levels within CdS nanostructures. These energy levels may help suppress electron-hole recombination and improve charge separation during photocatalytic reactions. It is worth mentioning that silicon has inherent potential to quench and promote excited electrons due to additional energy levels where these are progressively used in H^+ reduction[95]. Moreover, Si–dopants may contribute to improve charge transfer behaviour

View Article Online
DOI: 10.1039/D6MA00439C

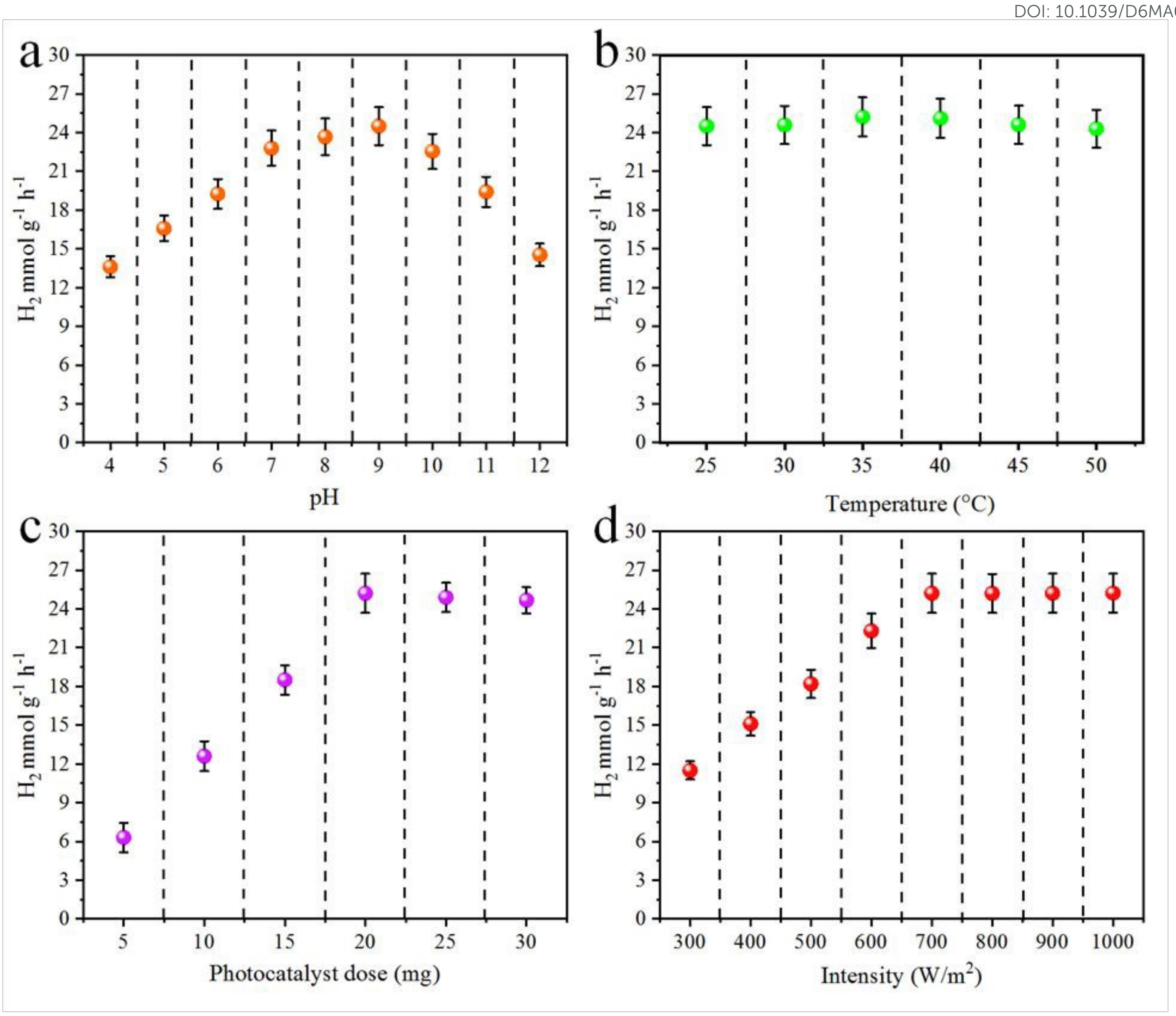

Fig.9: Illustrates the effect of factors (a) pH, (b) temperature, (c) catalysts dose and (d) represents the influence of light intensity on the activity of catalyst.

and facilitate water reduction reactions[96]. During the photoreaction, Cu cocatalysts may contribute to enhanced surface electron density and improved visible light utilization. The enhanced surface electron density may facilitate electron participation in water reduction reactions[97, 98]. Additionally, Cu loading may promote interfacial charge separation through possible Schottky-type interactions at the Cu/CdS interface[99]. The Mott-Schottky results suggest possible modulation of the electronic structure and flat band potential after Cu loading and Si incorporation [100] (Fig S3). As energetic electrons reach to more negative potentials, they become available for H^+ reduction and enhance hydrogen evolution. These electronic modifications may improve electron accumulation at catalytic reduction sites. Moreover, the combined presence of Cu and Si may enhance visible light harvesting and improve photocatalytic hydrogen evolution performance on Cu@Si–CdS system. On the basis of catalytic activities, it has been justified that Si dopants are essential to help out restrict the charges recombination and enhance the stability of CdS catalysts[101]. This work highlights the effectiveness of Cu@Si–CdS catalysts for sustainable hydrogen generation.

Factors influencing photocatalytic activity

The hydrogen evolution performance of photocatalysts is governed by a range of intrinsic and extrinsic parameters. In the present study, the effects of key operational variables–including reaction

DOI: 10.1039/D6MA00439C

temperature, light intensity, solution pH and catalysts dosage–were systematically examined to evaluate their influence on photocatalytic hydrogen generation. Furthermore, role of sacrificial reagents and impact of bandgap also revealed in the supporting information section. For the interest, several photoreactions were carried out to optimize these factors. Factors affecting catalytic activity have been discussed in supporting information section whereas figure associated with these factors has been described in main manuscripts; see Fig. 9.

Conclusion

In summary, CdS, Si-CdS, and Cu@Si–CdS photocatalysts were successfully prepared and investigated for hydrogen generation through photocatalytic water splitting reactions. All catalysts were synthesised using a combination of hydrothermal and chemical reduction techniques. The structural, morphological and optical properties of the catalysts were examined using XRD, Raman spectroscopy, SEM, AFM, UV–VIS/DRS, PL and VSM. Elemental composition and chemical states were confirmed through EDX and XPS analyses. Photocatalytic hydrogen evolution experiments were conducted in a 140 mL glass reactor (Velp-Sci), and hydrogen production was quantified using gas chromatograph equipped with a thermal conductivity detector accessory (GC–TCD). The results demonstrated that the incorporation of silicon dopants and copper cocatalysts effectively suppressed charge carrier recombination in the CdS system. Among the investigated materials, Cu@Si–CdS catalyst exhibited superior performances, achieving a hydrogen evolution rate of 23.85 mmol g^{-1} h^{-1} under similar conditions, which is approximately 6 times higher than that of pristine CdS. Higher H_2 production were accredited to both Si dopants and Cu–cocatalysts. Cu cocatalysts develop LSPR electrons and schottky junctions that prevent back reaction (i.e. recombination of charges). During the photoreactions, Si dopants facilitate the transfer of electrons towards redox sites by contributing additional energy levels to promote hydrogen evolution. Thus, higher charge transfer and less recombination is the significant factor to improved H_2 evolution with Cu@Si–CdS catalysts. The optimal reaction conditions were established at a temperature of 35 °C, pH 9, a light intensity of 700 W/m^2 and a catalyst loading of 20 mg in 25 mL of reaction mixture. Based on the observed performance and catalytic efficiencies, the material developed in this study demonstrate strong potential as alternatives to conventional catalysts that are commonly employed in hydrogen production technologies.

Conflict of interests

All authors have declared no financial interests.

Acknowledgement

This research was financially supported by the Higher Education Commission (HEC), Pakistan, under postdoctoral research grant Ref. 4-1/PDFP/HEC/2025(B-4)/33064/002 and ASIP research support. Additional funding was provided by Prince Sattam Bin Abdulaziz University through project No. PSAU/2026/R/1446. The synthesis of catalysts and the hydrogen evolution experiments were conducted in Inorganic Material Laboratory (52s), Institute of Chemistry, The Islamia University of Bahawalpur. Dr. Ejaz Hussain thanks Carnegie Mellon University for providing characterizations facility.

References

1. M. Jalil, K. Rafiq, M. Z. Abid, A. Rauf, S. Wang, S. Iqbal and E. Hussain, Nanoscale Advances, 2023, 5, 3233-3246.
2. B. Changmai, C. Vanlalveni, A. P. Ingle, R. Bhagat and S. L. Rokhum, RSC advances, 2020, 10, 41625-41679.
3. A. Goeppert, M. Czaun, G. S. Prakash and G. A. Olah, Energy & Environmental Science, 2012, 5, 7833-7853.
4. M. E. Scofield, H. Liu and S. S. Wong, Chemical Society Reviews, 2015, 44, 5836-5860.
5. J. Cai, L. Li, X. Lv, C. Yang and X. Zhao, ACS Applied Materials & Interfaces, 2014, 6, 167-175.
6. D. V. Esposito, I. Levin, T. P. Moffat and A. A. Talin, Nature materials, 2013, 12, 562-568.
7. P.-A. Le, V. D. Trung, P. L. Nguyen, T. V. B. Phung, J. Natsuki and T. Natsuki, RSC advances, 2023, 13, 28262-28287.
8. A. Basile and T. Napporn, 2020.
9. K. U. Sahar, K. Rafiq, M. Z. Abid, U. ur Rehman, A. Rauf and E. Hussain, Reaction Chemistry & Engineering, 2023, 8, 2522-2536.
10. M. Sabir, K. Rafiq, M. Z. Abid, U. Quyyum, S. S. A. Shah, M. Faizan, A. Rauf, S. Iqbal and E. Hussain, Fuel, 2023, 353, 129196.
11. Z. Abid, K. Rafiq, A. Rauf, R. H. Althomali and E. Hussain, Materials Advances, 2024.
12. F. Tezcan, A. Ahmad, G. Yerlikaya, H. Paksoy and G. Kardaş, New Journal of Chemistry, 2022, 46, 9290-9297.
13. J. Abdul Nasir, A. Munir, N. Ahmad, T. u. Haq, Z. Khan and Z. Rehman, Advanced Materials, 2021, 33, 2105195.
14. J. A. Nasir, Z. ur Rehman, S. N. A. Shah, A. Khan, I. S. Butler and C. R. A. Catlow, Journal of Materials Chemistry A, 2020, 8, 20752-20780.
15. S. Hussain, D. Vikraman, Z. Ali Sheikh, Z. Abbas, S. Aftab, G. Nazir, D.-K. Kim, H.-S. Kim and J. Jung, Renewable Energy, 2024, 228, 120645.

View Article Online
DOI: 10.1039/D6MA00430C

16. S. Hussain, D. Vikraman, Z. Abbas, M. Faizan, S. Aftab, K. M. Batoo, H.-S. Kim, K.-W. Nam and J. Jung, Sustainable Materials and Technologies, 2023, 37, e00696.
17. Z. Abbas, K. Fatima, S. H. Mirza, A. Parveen and S. Muhammad, Journal of Electroceramics, 2024, https://doi.org/10.1007/s10832-024-00369-7.
18. W. Guo, Y. Zhang, J. Tian, Z. Liu, B. Liu and J. Li, Nature Communications, 2025, 17, 983.
19. M. Meng, X. Wu, Q. Chai, H. Zhou, N. Qin, H. Yuan, S. Zhao, J. Liu and J. Li, Rare Metals, 2025, 44, 10271-10281.
20. S. A. Ansari, M. M. Khan, M. O. Ansari and M. H. Cho, New Journal of Chemistry, 2015, 39, 4708-4715.
21. D. E. Anderson, S. Balapangu, H. N. Fleischer, R. A. Viade, F. D. Krampa, P. Kanyong, G. A. Awandare and E. K. Tiburu, Sensors, 2017, 17, 1831.
22. S. Chandrasekaran, L. Yao, L. Deng, C. Bowen, Y. Zhang, S. Chen, Z. Lin, F. Peng and P. Zhang, Chemical Society Reviews, 2019, 48, 4178-4280.
23. R. Kumar, W. Zheng, X. Liu, J. Zhang and M. Kumar, Advanced Materials Technologies, 2020, 5, 1901062.
24. N. Wajid, K. Rafiq, M. Z. Abid, A. Ilyas, T. Najam, A. Rauf and E. Hussain, Materials Chemistry and Physics, 2023, 306, 128062.
25. X. Meng, S. Wang, C. Zhang, C. Dong, R. Li, B. Li, Q. Wang and Y. Ding, Acs Catalysis, 2022, 12, 10115-10126.
26. J.-X. Lv, Z.-M. Zhang, J. Wang, X.-L. Lu, W. Zhang and T.-B. Lu, ACS applied materials & interfaces, 2018, 11, 2655-2661.
27. M. Z. Abid, K. Rafiq, A. Aslam, R. Jin and E. Hussain, Journal of Materials Chemistry A, 2024, 12, 7351-7395.
28. F. Ahmad, K. Rafiq, T. Najam, E. Hussain, M. Sohail, M. Z. Abid, A. Mahmood, M. S. Javed and S. S. A. Shah, International Journal of Hydrogen Energy, 2023, 48, 35075-35111.
29. K. Rafiq, M. Sabir, M. Z. Abid, M. Jalil, M. A. Nadeem, S. Iqbal, A. Rauf and E. Hussain, Energy & Fuels, 2024, 38, 4625-4636.
30. T. W. van Deelen, C. Hernández Mejía and K. P. de Jong, Nature Catalysis, 2019, 2, 955-970.
31. E. Hussain, I. Majeed, M. A. Nadeem, A. Badshah, Y. Chen, M. A. Nadeem and R. Jin, The Journal of Physical Chemistry C, 2016, 120, 17205-17213.
32. M. R. Khan, T. W. Chuan, A. Yousuf, M. Chowdhury and C. K. Cheng, Catalysis Science & Technology, 2015, 5, 2522-2531.
33. F. Saleem, M. Z. Abid, K. Rafiq, A. Rauf, K. Ahmad, S. Iqbal, R. Jin and E. Hussain, International Journal of Hydrogen Energy, 2024, 52, 305-319.
34. E. Hussain, A. Ishaq, M. Z. Abid, M. Z. Waleed, A. Rauf, R. Jin and K. Rafiq, ACS Applied Energy Materials, 2024, 7, 1914-1926.
35. S. Sarina, E. R. Waclawik and H. Zhu, Green chemistry, 2013, 15, 1814-1833.
36. J. A. Nasir, N. Islam, Z. ur Rehman, I. S. Butler, A. Munir and Y. Nishina, Materials Chemistry and Physics, 2021, 259, 124140.
37. J. Nie, A. Patrocinio, S. Hamid, F. Sieland, J. Sann, S. Xia, D. Bahnemann and J. Schneider, Physical Chemistry Chemical Physics, 2018, 20, 5264-5273.
38. J. Jin, Y. Cao, T. Feng, Y. Li, R. Wang, K. Zhao, W. Wang, B. Dong and L. Cao, Catalysis Science & Technology, 2021, 11, 2753-2761.
39. J. A. Nasir, M. Hafeez, M. Arshad, N. Z. Ali, I. F. Teixeira, I. McPherson and M. A. Khan, ChemSusChem, 2018, 11, 2587-2592.
40. X. Fu, Y. Zhang, S. Yang, Q. Chai, Z. Liu, H. Wang, K. Wang, Z. Zhao, N. Li, H. Huang and J. Li, ACS Catalysis, 2026, 16, 1091-1102.
41. P. Wang, S. Zhan, H. Wang, Y. Xia, Q. Hou, Q. Zhou, Y. Li and R. R. Kumar, Applied Catalysis B: Environmental, 2018, 230, 210-219.
42. S. Azmi, P. Jamal and A. Amid, International Food Research Journal, 2012, 19.
43. D. G. Gizaw, S. Periyasamy, Z. T. Redda, B. I. John, H. Baylie Mengstie and P. Asaithambi, Environmental Quality Management, 2023.
44. P. M. Valencia, P. A. Basto, L. Zhang, M. Rhee, R. Langer, O. C. Farokhzad and R. Karnik, ACS nano, 2010, 4, 1671-1679.
45. T. Hisatomi and K. Domen, Nature Catalysis, 2019, 2, 387-399.
46. B. Bulfin, L. Buttsworth, A. Lidor and A. Steinfeld, Chemical Engineering Journal, 2021, 421, 127734.
47. Y. Zhang, J. Guo, J. Zhang, X. Qiu, X. Zhang, J. Han, B. Zhang, C. Long, Y. Shi and Z. Yang, Chem, 2022, 8, 1688-1704.
48. L. Riccardi, Technische Universiteit Eindhoven, 2023.
49. M. Z. Rahman, M. G. Kibria and C. B. Mullins, Chemical Society Reviews, 2020, 49, 1887-1931.
50. S. E. Salas, B. S. Rosales and H. de Lasa, Applied Catalysis B: Environmental, 2013, 140, 523-536.
51. H. Ullah, E. Viglašová and M. Galamboš, Processes, 2021, 9, 263.
52. T. N. Blanton and D. Majumdar, Powder Diffraction, 2012, 27, 104-107.
53. M. Muthusamy, S. Muthukumaran and M. Ashokkumar, Ceramics International, 2014, 40, 10657-10666.
54. M. F. Iqbal, S. Saeed, L. Wu, P. Zhu and D. Wang, Journal of Raman Spectroscopy, 2019, 50, 1492-1501.
55. J. Wang, M. Wang, J. Shi, Y. Zhou, C. Zhang and A. S. Bhatti, Journal of Alloys and Compounds, 2023, 944, 169063.
56. X. Xu, A. Dutta, J. Khurgin, A. Wei, V. M. Shalaev and A. Boltasseva, Laser & Photonics Reviews, 2020, 14, 1900376.
57. N. T. M. Duc, H. Srikanth and M.-H. Phan, Science and Technology of Advanced Materials, 2025, 26, 2546287.
58. A. Almohammedi, Applied Physics A, 2023, 129, 221.
59. W. Li, F. Wang, X.-y. Liu, Y.-y. Dang, J.-y. Li, T.-h. Ma and C.-y. Wang, Applied Catalysis B: Environmental, 2022, 313, 121470.
60. C. Byrne, G. Subramanian and S. C. Pillai, Journal of environmental chemical engineering, 2018, 6, 3531-3555.
61. A. Yurtsever, P.-X. Wang, F. Priante, Y. Morais Jaques, K. Miyazawa, M. J. MacLachlan, A. S. Foster and T. Fukuma, Science Advances, 2022, 8, eabq0160.
62. E. Hussain, M. Jalil, Z. Abid, J. Mansab, R. Hamed Althomali, S. Wang, A. Rauf and K. Rafiq, Materials Advances, 2024, https://doi.org/10.1039/D3MA01137B.
63. Z. Abid, K. Rafiq, A. Rauf and E. Hussain, Nanoscale Advances, 2024.
64. M. Tong, D. Sun, R. Zhang, H. Liu and R. Chen, Journal of Alloys and Compounds, 2021, 862, 158271.
65. E. Hussain, M. Sultana, M. Z. Abid, A. K. Buzdar, H. K. Thabet, S. M. El-Bahy, M. Jalil, A. Rauf, Z. M. El-Bahy and

K. Rafiq, Environmental Science: Water Research & Technology, 2024, https://doi.org/10.1039/D4EW00300D.
66. G. Zheng, Y. Xiang, L. Xu, H. Luo, B. Wang, Y. Liu, X. Han, W. Zhao, S. Chen, H. Chen, Q. Zhang, T. Zhu and Y. Yang, Advanced Energy Materials, 2018, 8, 1801718.
67. E. Hussain, M. Jalil, Z. Abid, J. Mansab, R. H. Althomali, S. Wang, A. Rauf and K. Rafiq, Materials Advances, 2024.
68. Y. Naciri, A. Hsini, Z. Ajmal, A. Bouddouch, B. Bakiz, J. Navío, A. Albourine, J. Valmalette, M. Ezahri and A. Benlhachemi, Journal of colloid and interface science, 2020, 572, 269-280.
69. M. Shkir, I. Ashraf, S. AlFaify, A. M. El-Toni, M. Ahmed and A. Khan, Ceramics International, 2020, 46, 4652-4663.
70. M. Ikram, M. Rashid, A. Haider, S. Naz, J. Haider, A. Raza, M. Ansar, M. K. Uddin, N. M. Ali and S. S. Ahmed, Sustainable Materials and Technologies, 2021, 30, e00343.
71. V. Arun, V. Manikandan, M. S. AlSalhi, S. Devanesan, A. Priyadharsan, R. K. KA and P. Maadeswaran, Chemosphere, 2022, 300, 134460.
72. V. Kumar, N. Nisika and M. Kumar, Advanced Optical Materials, 2021, 9, 2001150.
73. B. Thangaraj, P. R. Solomon and S. Ranganathan, Current pharmaceutical design, 2019, 25, 1455-1476.
74. A. Kleiman-Shwarsctein, P. Zhang, Y. Hu and E. W. McFarland, On solar hydrogen & nanotechnology, 2010, 399-458.
75. A. Yan, X. Shi, F. Huang, M. Fujitsuka and T. Majima, Applied Catalysis B: Environmental, 2019, 250, 163-170.
76. Y. Hu, X. Hao, Z. Cui, J. Zhou, S. Chu, Y. Wang and Z. Zou, Applied Catalysis B: Environmental, 2020, 260, 118131.
77. W. Xu, W. Tian, L. Meng, F. Cao and L. Li, Advanced Energy Materials, 2021, 11, 2003500.
78. K. Zhang, R. Wang, X. Zhong and F. Jiang, ACS Omega, 2024.
79. M. Z. Abid, K. Rafiq, A. Rauf, R. H. Althomali, R. Jin and E. Hussain, Renewable Energy, 2024, 225, 120223.
80. V. Kumaravel, M. D. Imam, A. Badreldin, R. K. Chava, J. Y. Do, M. Kang and A. Abdel-Wahab, Catalysts, 2019, 9, 276.
81. W. Septina, R. R. Prabhakar, R. Wick, T. Moehl and S. D. Tilley, Chemistry of Materials, 2017, 29, 1735-1743.
82. P. Babu, S. R. Dash, A. Behera, T. Vijayaraghavan, A. Ashok and K. Parida, Nanoscale Advances, 2022, 4, 150-162.
83. G. De, A. Roy and S. Bhattacharya, International journal of hydrogen energy, 1995, 20, 127-131.
84. H. Park, W. Choi and M. R. Hoffmann, Journal of Materials Chemistry, 2008, 18, 2379-2385.
85. Z. Khan, M. Khannam, N. Vinothkumar, M. De and M. Qureshi, Journal of Materials Chemistry, 2012, 22, 12090-12095.
86. X. Wang, G. Liu, G. Q. Lu and H.-M. Cheng, international journal of hydrogen energy, 2010, 35, 8199-8205.
87. X. Ding, Y. Li, J. Zhao, Y. Zhu, Y. Li, W. Deng and C. Wang, APL Materials, 2015, 3, 104410.
88. X. Chen, W. Chen, H. Gao, Y. Yang and W. Shangguan, Applied Catalysis B: Environmental, 2014, 152, 68-72.
89. J. Zhang, S. Z. Qiao, L. Qi and J. Yu, Physical chemistry chemical physics, 2013, 15, 12088-12094.
90. N. Biswal, D. Das, S. Martha and K. Parida, international journal of hydrogen energy, 2011, 36, 13452-13460.
91. S. Chen, D. Huang, P. Xu, W. Xue, L. Lei, M. Cheng, R. Wang, X. Liu and R. Deng, Journal of Materials Chemistry A, 2020, 8, 2286-2322.
92. P. Cavaliere, in *Water Electrolysis for Hydrogen Production*, Springer, 2023, pp. 105-157.
93. R. M. Navarro Yerga, M. C. Álvarez Galván, F. Del Valle, J. A. Villoria de la Mano and J. L. Fierro, ChemSusChem: Chemistry & Sustainability Energy & Materials, 2009, 2, 471-485.
94. U. Quyyum, K. Rafiq, M. Z. Abid, F. Ahmad, A. Rauf and E. Hussain, Environmental Science: Water Research & Technology, 2023, 9, 1147-1160.
95. X. Wang, L. Ge, K. Wei, Z. Xing and S. Feng, International Journal of Hydrogen Energy, 2024, 55, 718-728.
96. A. Jena, C.-J. Chen, H. Chang, S.-F. Hu and R.-S. Liu, Journal of Materials Chemistry A, 2021, 9, 3767-3785.
97. Y. Liu, Y.-X. Yu and W.-D. Zhang, The Journal of Physical Chemistry C, 2013, 117, 12949-12957.
98. Z. Li, T. Yan and X. Fang, Nature Reviews Materials, 2023, 8, 587-603.
99. R. L. McCreery, J. Wu and R. P. Kalakodimi, Physical Chemistry Chemical Physics, 2006, 8, 2572-2590.
100. A. F. Gualdrón-Reyes, A. M. Meléndez, J. Tirado, M. A. Mejia-Escobar, F. Jaramillo and M. E. Niño-Gómez, Nanoscale, 2019, 11, 762-774.
101. H. Eidsvåg, S. Bentouba, P. Vajeeston, S. Yohi and D. Velauthapillai, Molecules, 2021, 26, 1687.

View Article Online
DOI: 10.1039/D6MA00439C

Data Availability Statement

The data and necessary protocols of this study have been included as part of the Supplementary Information.